SPONSORED BY R&D SYSTEMS INC.

www.rndsystems.com/pathways

Contribution of Semi-Arid Forests to the Climate System

Eyal Rotenberg and Dan Yakir

Science **327**, 451 (2010);
DOI: 10.1126/science.1179998

This copy is for your personal, non-commercial use only.

If you wish to distribute this article to others, you can order high-quality copies for your colleagues, clients, or customers by clicking here.

Permission to republish or repurpose articles or portions of articles can be obtained by following the guidelines here.

The following resources related to this article are available online at www.sciencemag.org (this information is current as of November 23, 2012):

Updated information and services, including high-resolution figures, can be found in the online version of this article at:
http://www.sciencemag.org/content/327/5964/451.full.html

A list of selected additional articles on the Science Web sites **related to this article** can be found at:
http://www.sciencemag.org/content/327/5964/451.full.html#related

This article **cites 33 articles**, 7 of which can be accessed free:
http://www.sciencemag.org/content/327/5964/451.full.html#ref-list-1

This article has been **cited by** 1 article(s) on the ISI Web of Science

This article has been **cited by** 4 articles hosted by HighWire Press; see:
http://www.sciencemag.org/content/327/5964/451.full.html#related-urls

This article appears in the following **subject collections:**
Atmospheric Science
http://www.sciencemag.org/cgi/collection/atmos

Downloaded from www.sciencemag.org on November 23, 2012

Science (print ISSN 0036-8075; online ISSN 1095-9203) is published weekly, except the last week in December, by the American Association for the Advancement of Science, 1200 New York Avenue NW, Washington, DC 20005. Copyright 2010 by the American Association for the Advancement of Science; all rights reserved. The title *Science* is a registered trademark of AAAS.

Our findings also have implications for precise dating of early events in the history of the solar system. The Pb-Pb age equation (Eq. 1) has been used for decades to calculate the absolute ages of both meteoritic and terrestrial materials (*24*). This equation assumes that $^{238}U/^{235}U$ is invariant at any given time, and that the present-day value is 137.88.

$$\frac{^{206}Pb^*}{^{206}Pb^*} = \frac{^{235}U e^{\lambda_{235}t} - 1}{^{238}U e^{\lambda_{238}t} - 1} = \frac{1}{137.88}\frac{e^{\lambda_{235}t} - 1}{e^{\lambda_{238}t} - 1} \quad (1)$$

Here, λ is the decay constant for the specific isotope and t is the age. Any deviation from this assumed $^{238}U/^{235}U$ would cause miscalculation in the determined Pb-Pb age of a sample. A difference of up to 3.5 per mil (‰) implies that a correction of up to –5 My would be required if the Pb-Pb ages of these CAIs were obtained using the previously assumed $^{238}U/^{235}U$ value (Fig. 4).

Because $^{238}U/^{235}U$ variations in solar system materials are not restricted to CAIs, this requirement may extend to high-precision Pb-Pb dating of other materials as well. It is possible, however, that the $^{238}U/^{235}U$ values of bulk chondrites are controlled to a substantial degree by CAIs, which may be heterogeneously distributed at the scale at which these analyses were made.

The Pb-Pb dating technique is the only absolute dating technique able to resolve age differences of <1 My in materials formed in the early solar system. Whereas the full range of $^{238}U/^{235}U$ ratios reported here would result in an overestimation of the ages of these CAIs by up to 5 My, the largest excesses (>3.5‰) in ^{235}U occur in the group II CAIs that appear to have experienced the largest Cm/U fractionation. For non–group II CAIs, the age overestimation is ≤1 My. The apparent discrepancies between absolute Pb-Pb ages and relative (for example, ^{26}Al-^{26}Mg, ^{53}Mn-^{53}Cr, and ^{182}Hf-^{182}W) ages (*2*, *4*, *25*, *26*) may therefore place limits on the uncertainty of the age of the solar system.

References and Notes

1. C. M. Gray, D. A. Papanastassiou, G. J. Wasserburg, *Icarus* **20**, 213 (1973).
2. Y. Amelin, A. N. Krot, I. D. Hutcheon, A. A. Ulyanov, *Science* **297**, 1678 (2002).
3. A. Bouvier, J. Blichert-Toft, F. Moynier, J. D. Vervoort, F. Albarede, *Geochim. Cosmochim. Acta* **71**, 1583 (2007).
4. B. Jacobsen *et al.*, *Earth Planet. Sci. Lett.* **272**, 353 (2008).
5. J. Chen, G. J. Wasserburg, *Geophys. Res. Lett.* **7**, 275 (1980).
6. C. H. Stirling, M. B. Anderson, E.-K. Potter, A. Halliday, *Earth Planet. Sci. Lett.* **264**, 208 (2007).
7. S. Weyer *et al.*, *Geochim. Cosmochim. Acta* **72**, 345 (2008).
8. J. W. Arden, *Nature* **269**, 788 (1977).
9. M. Tatsumoto, T. Shimamura, *Nature* **286**, 118 (1980).
10. G. W. Lugmair, S. J. G. Galer, *Geochim. Cosmochim. Acta* **56**, 1673 (1992).
11. C. H. Stirling, A. N. Halliday, D. Porcelli, *Geochim. Cosmochim. Acta* **69**, 1059 (2005).
12. J. Chen, G. J. Wasserburg, *Earth Planet. Sci. Lett.* **52**, 1 (1981).
13. L. R. Nittler, N. Dauphas, *Meteorites and the Early Solar System II*, D. S. Lauretta, H. Y. McSween Jr., Eds. (Univ. of Arizona Press, Tucson, AZ, 2006), pp. 127–146.
14. W. V. Boynton, *Earth Planet. Sci. Lett.* **40**, 63 (1978).
15. G. J. Wasserburg, M. Busso, R. Gallino, *Astrophys. J.* **466**, L109 (1996).
16. G. J. Wasserburg, M. Busso, R. Gallino, K. M. Nollet, *Nucl. Phys.* **777**, 5 (2006).
17. T. Shimamura, G. W. Lugmair, *Lunar Planet. Sci.* **XII**, 976 (1981).
18. Materials and methods are available as supporting material on *Science* Online.
19. J. B. Blake, D. N. Schramm, *Nature* **289**, 138 (1973).
20. G. J. MacPherson, *Treatise on Geochemistry, Volume 1* A. M. Davis, Ed. (Elsevier, Amsterdam, 2003), pp. 201–246.
21. W. V. Boynton, *Geochim. Cosmochim. Acta* **39**, 569 (1975).
22. A. M. Davis, L. Grossman, *Geochim. Cosmochim. Acta* **43**, 1611 (1979).
23. B. Mason, S. R. Taylor, *Contributions to the Earth Sciences*, vol. 25 (Smithsonian Institution Scholarly Press, Washington, DC, 1982).
24. C. C. Patterson, *Geochim. Cosmochim. Acta* **10**, 230 (1956).
25. G. W. Lugmair, A. Shukolyukov, *Geochim. Cosmochim. Acta* **62**, 2863 (1998).
26. C. Burkhardt *et al.*, *Geochim. Cosmochim. Acta* **72**, 6177 (2008).

27. We thank the Center for Meteorite Studies at Arizona State University and the Senckenberg Museum in Frankfurt for providing the samples. We thank the W. M. Keck Laboratory for Environmental Biogeochemistry and R. Hines for technical assistance. We are grateful to H. Palme for helpful discussions and to R. Williams and L. Borg for assistance with the double spike. We also thank G. Wasserburg, S. Galer, and an anonymous reviewer for thoughtful comments that greatly improved the manuscript. This work was partially supported by NASA Origins of Solar Systems grant NNX07AF49G to M.W., as well as NASA Astrobiology Institute grant NNA09DA79A and NASA Exobiology Program grant NNX07AU15G to A.D.A.

Supporting Online Material

www.sciencemag.org/cgi/content/full/science.1180871/DC1
Materials and Methods
Fig. S1
Tables S1 and S2
References

20 August 2009; accepted 11 December 2009
Published online 31 December 2009;
10.1126/science.1180871
Include this information when citing this paper.

Downloaded from www.sciencemag.org on November 23, 2012

Contribution of Semi-Arid Forests to the Climate System

Eyal Rotenberg and Dan Yakir*

Forests both take up CO_2 and enhance absorption of solar radiation, with contrasting effects on global temperature. Based on a 9-year study in the forests' dry timberline, we show that substantial carbon sequestration (cooling effect) is maintained in the large dry transition zone (precipitation from 200 to 600 millimeters) by shifts in peak photosynthetic activities from summer to early spring, and this is counteracted by longwave radiation (*L*) suppression (warming effect), doubling the forestation shortwave (*S*) albedo effect. Several decades of carbon accumulation are required to balance the twofold *S* + *L* effect. Desertification over the past several decades, however, contributed negative forcing at Earth's surface equivalent to ~20% of the global anthropogenic CO_2 effect over the same period, moderating warming trends.

The need to generate measurement-based estimates of biosphere-atmosphere carbon and energy exchange on land (*1*, *2*) led to global observational efforts to measure the carbon, water, and radiation fluxes at the canopy scale (www.fluxnet.ornl.gov). Obtaining primary data from semi-arid regions is important principally because of their size [2.4 billion ha or ~17.7% of total land surface area (*3*)] coupled with their low clouds–high solar radiation conditions: 18 to 21 and 10 to 13 MJ m^{-2} day^{-1} in semi-arid and temperate regions, respectively (*4*). These regions have potentially large impacts on local climate (*5*–*7*) and the global radiation budget and represent climatic conditions predicted for large areas of currently wetter regions (*8*). We used the concept of "radiative forcing" as a metric for comparing changes in surface energy balance with carbon uptake and storage associated with semi-arid forestation.

We used a field research site with continuous flux measurements of CO_2, water vapor, and energy established in 2000 in a 2800-ha pine forest (Yatir) in southern Israel, using methodology established in the Euroflux network (*9*). The forest represents a low-stature (10 m), low-density [leaf area index (LAI) ~ 1.3] woody vegetation ecosystem at the dry timberline (285 mm mean precipitation). The forest maintains relatively high productivity, with a mean annual net ecosystem CO_2 exchange (*NEE*) of 2.3 ton C ha^{-1} for the study period (*10*), compared with ~2.0 ton C ha^{-1} in European pine forests and a Fluxnet mean of ~2.5 ton C ha^{-1} (Table 1). This reflects moderate mean annual gross primary productivity (*GPP*) coupled with low mean annual

Environmental Sciences and Energy Research, Weizmann Institute of Science, Rehovot 76100, Israel.

*To whom correspondence should be addressed. E-mail: dan.yakir@weizmann.ac.il

carbon loss in respiration (R_e), resulting in a high *NEE*/*GPP* ratio (Table 1).

The indicators of high carbon use efficiency are associated with a range of eco-physiological adjustments (*11*), as well as potential increase in fire hazard (*12*). The most fundamental adjustment is the "homeostatic-like" stability in ambient conditions during time of peak activity reported in Fig. 1. Moving from the northern (Finland) to the southern (Israel) pine forest sites, time of peak GPP shifts from July and August to mid-March, narrowing down substantially the climatic gradient, such as in air temperature from 17.4°C (annual mean) to 4.6°C (time of peak GPP, when mean temperature is 17.0° ± 1.5°C, excluding one outlier maritime site), or in incoming global irradiance (E_g, from 150 W m^{-2} annual mean to 67 W m^{-2} for time of peak GPP). For a first approximation, the change in day of year of peak GPP (DOY_{GPP}) is best described by the gradient in annual mean E_g: $DOY_{GPP} = -0.71(E_g) + 263.1$ ($R^2 = 0.87$), or 7 days advance for each increase of 10 W m^{-2} in annual mean global radiation. The trend depicted in Fig. 1 is for European pine forests, reflecting plasticity within a single vegetation type rather than changes in species composition along geographical and climatic gradients (*13*). This homeostatic-like ecosystem-scale behavior also provides an alternative perspective to the proposed leaf-level "homeostatic" temperature reconstructed from oxygen isotopic records in plant matter (*14*).

The adjustments in timing and productivity noted above provide a contrasting and more optimistic long-term view of forest productivity and carbon uptake than those based on episodic droughts in temperate climates. For example, signature drought years like 2003 in Europe (*15*) indicated massive losses of carbon from forest ecosystems, but the results here indicate that long-term management of forestation can result in productive forests that can sustain seasonal drought permanently (*10*).

In addition to carbon, we must consider the direct effects of vegetation cover on the surface radiation balance (*2*, *16*, *17*), where the semi-arid forest also indicates large effects. From a global prospective, the characteristics of energy fluxes over a semi-arid forest such as Yatir are unique (Fig. 2). The incoming solar radiation approaches that of the Sahara, but owing to an albedo as low as in other forests the net radiation (R_n) is higher than that in any of the other eco-regions (35% greater than in the Sahara). The high net radiation coupled with the dry environment (small latent heat flux; Fig. 2 inset) results in a sensible heat flux, H, larger than that of any of the other eco-regions (30% larger than the Sahara and 1.6 and 2.4 times greater than tropical and temperate forests, respectively). Two important implications are, first, that the albedo change associated with forestation in the low-cloud high-radiation environment results in a large increase in surface radiation load. We observed (*18*) a 0.1 change (decrease) in mean albedo (δ_α) above the forest compared with that above the sparse background shrubland [compare with (*19*–*21*)]. Combined with the high global radiation, this δ_α yields a large increase in annual shortwave radiation load of δ_S = +23.8 W m^{-2}. Second, we report that this relatively large shortwave albedo effect (*16*, *17*, *22*) is essentially doubled by a longwave radiation effect.

With suppressed latent heat flux (*LE*) because of lack of water, the forest is transformed into an effective "convector" that exploits the low tree density and open canopy and, consequently, high canopy-atmosphere aerodynamic coupling. Indeed, low aerodynamic resistance (r_a) was estimated [~16 s m^{-1} annual mean midday value (*23*)] supporting the massive H (Fig. 2 inset). This is associated with a large increase in surface roughness in going from shrubland to forest, resulting in changes in buoyancy and increasing efficiency of heat convection, with potential implications on local circulation.

The effective convector effect of the canopy-atmosphere coupling resulted in annual mean cooling of the canopy surface temperature of about 5°C, compared with that of the background shrubland (and as much as a 30°C cooling in summer midday). This was associated with high Bowen ratio ($\beta = H/LE$), which was on average 5.2 (>10 in summer). In contrast, in temperate and tropical forests the albedo-related increased radiation load is typically compensated for by evapotranspiration, reducing temperature differences between forest and nonforest surfaces and maintaining β around 1.

Longwave radiation is of great importance in the semi-arid system (*20*, *24*). And a consequence of the surface cooling in the forested area is a suppression of the upwelling longwave radiation flux, L. In fact, the annual mean longwave radiation suppression that we observed (*18*) in our forest-shrubland comparison is δ_L ~ 25 W m^{-2} (up to 100 W m^{-2} in summer midday) and is equivalent in magnitude to the shortwave albedo effect (~23.8 W m^{-2}; Table 2). Therefore, in dry vegetation ecosystems the increase in surface radiation load is twice as large when both the shortwave, albedo, and the longwave radiation effects are considered (balanced by heat transfer to the overlaying boundary layer).

The surface energy characteristics in the semi-arid regions have at least two important global

Table 1. Indicators of carbon use efficiency in pine forests: *GPP*, R_e, and *NEE* of carbon for the 12 European pine forest sites [62 data years (*36*)], for the entire global Fluxnet network (*43*), and for semi-arid forest [Yatir (*44*)].

Pine forest	*GPP*	R_e	*NEE*	*NEE*/*GPP*
European (Carboeurope)	1142	944	200	0.17
Global (FluxNet)	1540	1280	260	0.17
Semi-arid (Yatir)	820	600	220	0.27

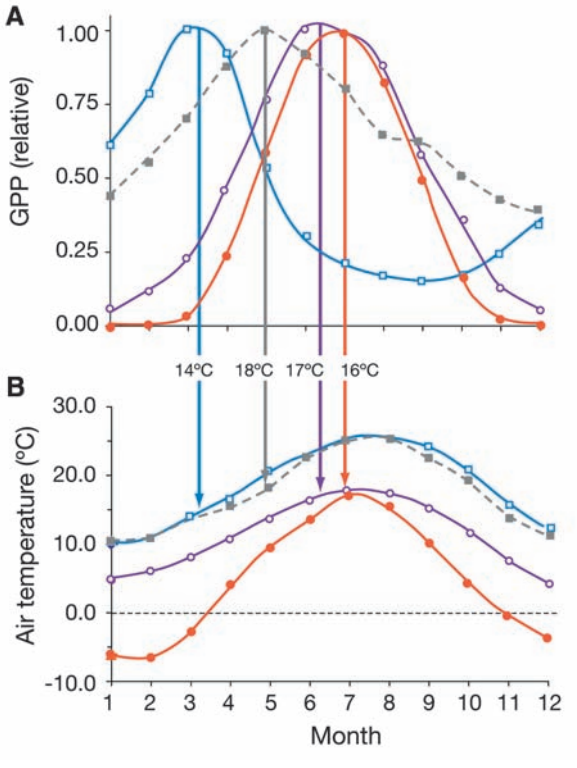

Fig. 1. Annual patterns in (**A**) GPP, monthly means based on 0.5-hour values from Carboeurope database (*36*) and normalized as GPP/GPP_{max}, and (**B**) air temperature (monthly mean) in 4 representative European pine forest sites (out of the 12 Carboeurope pine forest sites examined; other sites omitted for clarity but are within same range). Vertical lines indicate the air temperature at time of peak activity. Sites are Yatir, Israel (blue); El Salar, Spain (gray); Brasschaat, Belgium (purple); and Hyytiala, Finland (orange).

Downloaded from www.sciencemag.org on November 23, 2012

implications when considering the large land surface areas involved. First, the success of afforestation and the associated carbon sequestration potential must also be linked to the consequences in surface energy balance. Secondly, the results provide a basis for a first approximation of the impact of the large-scale desertification process that took place in the semi-arid region over the past several decades.

We used the observed albedo-derived shortwave radiative forcing (*RF*) of the forest, δ_S = +23.8, together with the calculated *RF* associated with carbon sequestration, using (*17*) and (*25*) and the observed semi-arid forest productivity [~2.3 ton C ha^{-1} annually (*10*) and ~100 ton C ha^{-1} over the past 40 years (*26*)] to estimate the time required to achieve balance between the two *RF* values (*27*). The *RF* values in this context should be interpreted with caution (*28*) and are used here as a convenient way to compare the magnitude of biogeophysical and biogeochemical forcing (*24*). The estimated time required to reach this balance in the semi-arid environment is ~40 years. Such calculation traditionally considers only the shortwave radiation effect. Explicitly introducing the observed longwave radiation suppression effect in this calculation doubles the time needed to achieve the *RF* balance, considering that δ_S and δ_L are similar (23.8 and 25 W m^{-2}).

Such estimates indicate that a net negative (cooling) *RF* is reached only after ~80 years of forestation, but we note that the data used here provide a "worst-case scenario" by considering results from the dry timberline and ignoring the possibly greater climate sensitivity to CO_2 removal than to land surface changes (*28*). Obtaining the full range of *RF*-C sequestration tipping points across the climate transition zone is important, will likely indicate much shorter mean time to reach a net cooling effect, and should also consider that afforestation of only ~12% of dry, carbon-neutral areas (*3*, *29*) can produce a carbon sink of ~1 Pg C year^{-1} for a minimum 50 years of forest growth. This is equivalent to one "wedge" to address potential anthropogenically derived climate change (*30*).

Lastly, we address the implications of our results for long-term desertification trends in the semi-arid region. From the atmospheric and surface radiation perspective, the Yatir forest provides a generic representation of vegetation of similar LAI in the semi-arid region [2.1 ± 1.6 and 1.3 ± 0.9 for shrubland and deserts (*31*)]. Such vegetation types underwent large-scale desertification over the past several decades, estimated at ~5.8 Mha year^{-1} (*3*, *32*). We estimated that the total organic carbon released from a fully degraded land surface is ~2.2 kg C m^{-2} (*3*, *29*, *33*) and that the degradation period (DP) for the release of carbon to the atmosphere is about 50 years. We consider the albedo effect, however, to peak in about half that time (~25 years) because it is associated only with live vegetation, whereas carbon degradation in litter and soil organic matter is not. Using the approach of (*17*) for the shortwave radiation (*S*) albedo effect but expanded to explicitly include the thermal radiation (*L*) suppression discussed above, we estimated the potential *RF* of the transition from vegetation cover with LAI of ~1.3 to near zero under semi-arid conditions as:

$$RF_{S+L}(y) = A(y)(\delta_\alpha \cdot E_g + \delta_L)/A_E \quad (1)$$

where $A(y)$ is the annually degraded area accumulated to year y (calculated as a time series with full degradation in 25 years), $\delta_\alpha = 0.1$, E_g = 240 W m^{-2}, $\delta_L = 25$ (Table 2), and A_E is Earth surface area (5.1 × 10^{14} m^2). This estimate indicates a negative (cooling) radiative forcing at the surface over a 35-year degradation process (say, 1970–2005 when data quoted above apply) of −0.145 W m^{-2} (−0.075 plus −0.070 W m^{-2} associated with *S* and *L*, respectively).

The radiative forcing resulting from the CO_2 released from biomass degradation associated with desertification can be estimated according to (*25*):

$$RF_{CO_2}(y) = \eta \cdot Ln\left[1 + \frac{C(y)}{C_0}\right] \quad (2)$$

where η is the CO_2 radiative forcing efficiency (5.35 W m^{-2}); C_0 is a reference CO_2 concentration (360 ppm); $C(y) = A(y)C\kappa/\zeta$ sums the total CO_2 emitted over y years [35 years of desertification in this case (*3*)]; $A(y)$ is as above with degradation period of 50 years, acknowledging the delay in degradation effects between surface radiation and CO_2 release; *C* is the total degradable carbon per unit land area (see above); κ converts kg of C to ppmv [2.13 × 10^{12} kg C per part per million by volume (ppmv^{-1})]; and ζ is the airborne fraction [0.5 (*34*)]. The results indicate that the releases of CO_2 to the atmosphere

Table 2. Annual mean values (6 years) of radiation fluxes, albedo, and surface (skin) temperature in the semi-arid forest (Yatir) and in the shrubland background.

Variable	Forest	Shrubland
Global radiation (E_g, W m^{-2})	238	238
Albedo (unit-less)	0.11	0.21
Net solar radiation (S_n, W m^{-2})	212	188
Net longwave radiation (L_n, W m^{-2})	−96	−121
Net radiation ($R_n = S_n + L_n$, W m^{-2})	115	67
Skin temperature (°C)	19	24*

*(*27*)

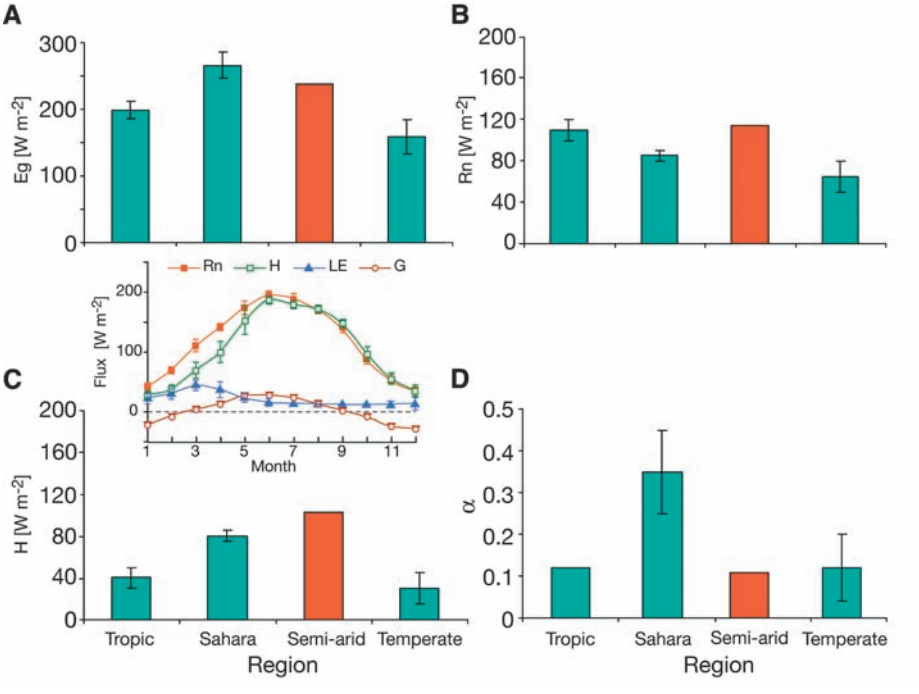

Fig. 2. Annual means of energy flux components in forests (except Sahara) in globally representative regions: **(A)** iE_g, **(B)** R_n, **(C)** *H*, and **(D)** surface albedo, α. Values for tropical forests include Africa and South America; temperate forests are represented by forests around latitude 45°N in North America and Europe; semi-arid forests are represented by Yatir (mean for the study period); the Sahara represents hot deserts. Error bars indicate the range in literature-reported values. Albedo values for tropical forests, the Sahara, and temperate forests are from (*37*–*41*). Values for E_g are from (*4*), and for R_n and *H* from (*42*). (Inset) The mean seasonal cycle in energy fluxes in the semi-arid Yatir forest during the study period.

Downloaded from www.sciencemag.org on November 23, 2012

during the above desertification period had radiative forcing of +0.006 W m^{-2}, a factor of 24 smaller and in the opposite direction than the combined radiative effects [compare with (*28*)].

On the basis of our estimates, the total desertification in the semi-arid regions had a combined *RF* of about –0.14 W m^{-2}. This counteracts the equivalent of ~20% of the global *RF* associated with the 44-ppmv increase in atmospheric CO_2 over the same period [(*35*) e.g., (0.145–0.006)/0.62; see Eqs. 1 and 2], moderating the potential warming trend. This moderating effect adds to that assigned to the low CO_2 airborne fraction resulting from ocean and land carbon sinks (*34*). These are clearly first approximations, but the large effects and the large area involved with generally stable high-radiation low-cloud conditions make these estimates relatively robust and demonstrate again the importance of research in the semi-arid regions.

References and Notes

1. D. Baldocchi *et al.*, *Bull. Am. Meteorol. Soc.* **82**, 2415 (2001).
2. G. B. Bonan, *Science* **320**, 1444 (2008).
3. R. Lal, *Environ. Manage.* **33**, 528 (2004).
4. National Climatic Data Center, "Mean daily solar radiation, monthly and annual" (U.S. Department of Commerce, Washington, DC, 1964).
5. J. Otterman, *Science* **186**, 531 (1974).
6. J. Charney, W. J. Quirk, S. H. Chow, J. Kornfield, *J. Atmos. Sci.* **34**, 1366 (1977).
7. Y. K. Xue, *Q. J. R. Meteorol. Soc.* **123**, 1483 (1997).
8. Intergovernmental Panel on Climate Change (IPCC), *Fourth Assessment Report, Climate Change 2007: Synthesis Report,* available at www.ipcc.ch/publications_and_data/publications_ipcc_fourth_assessment_report_synthesis_report.htm.
9. M. Aubinet *et al.*, *Adv. Ecol. Res* **30**, 113 (1999).
10. K. Maseyk, J. M. Grunzweig, E. Rotenberg, D. Yakir, *Glob. Change Biol.* **14**, 1553 (2008).
11. K. S. Maseyk *et al.*, *New Phytol.* **178**, 603 (2008).
12. D. M. J. S. Bowman *et al.*, *Science* **324**, 481 (2009).
13. J. Penuelas, M. Boada, *Glob. Change Biol.* **9**, 131 (2003).
14. B. R. Helliker, S. L. Richter, *Nature* **454**, 511 (2008).
15. P. Ciais *et al.*, *Nature* **437**, 529 (2005).
16. G. Bala *et al.*, *Proc. Natl. Acad. Sci. U.S.A.* **104**, 6550 (2007).
17. R. A. Betts, *Nature* **408**, 187 (2000).
18. Four pairs of shortwave (0.29 to 4.0 μm, Kipp and Zonen CM21) and longwave (4.0 to 100 μm, Eppley precision infrared radiometer) radiation sensors were used, two (multiple positions) for measuring down- and upwelling radiation ~5 m above the canopy (and ~4 m away from the flux tower) and two (multiple positions) below the canopy ~1.5 m above bare soil surface. The L sensors output (precision mode) was corrected for solar radiation by using the companion S sensor. Albedo was estimated, in addition, from Moderate Resolution Imaging Spectroradiometer (MODIS) data for the forest and surrounding area using a full-year dark and white sky in the visible and near-infrared (NIR) spectral ranges (www-modis.bu.edu/brdf/userguide/albedo.html).
19. J. Charney, *Q. J. R. Meteorol. Soc.* **101**, 193 (1975).
20. G. L. Smith, A. C. Wilber, S. K. Gupta, P. W. Stackhouse Jr., *J. Clim.* **15**, 1175 (2002).
21. K. Fraedrich, A. Kleidon, F. Lunkeit, *J. Clim.* **12**, 3156 (1999).
22. M. Schaeffer *et al.*, *Global Biogeochem. Cycles* **20**, GB2020 (2006).
23. Aerodynamic resistance, r_a, was estimated as $r_a = \frac{H}{\Delta T_a} C_p \rho$. C_p and ρ are the air heat capacity and density; *H* was continuously measured; canopy-to-air temperature gradient, ΔT_a, was estimated from continuous sonic anemometer measurements 9 m above the canopy; and canopy "skin" temperature was estimated from upwelling longwave radiation measurements both above the soil and the canopy. For comparing forest and surrounding shrubland, surface temperatures were based on soil temperature measurements in the forest and at the shrubland (only 1 year for the latter), as well as MODIS surface temperature products for the forest and the surrounding region (at 10 km–by–10 km grids, 8-days mean at 10 AM, January through August 2005). Comparing roughness height was based on (*45*).
24. M. Claussen, V. Brovkin, A. Ganopolski, *Geophys. Res. Lett.* **28**, 1011 (2001).
25. G. Myhre, E. J. Highwood, K. P. Shine, F. Stordal, *Geophys. Res. Lett.* **25**, 2715 (1998).
26. A. Bar Massada, Y. Carmel, G. E. Tzur, J. M. Grünzweig, D. Yakir, *Can. J. For. Res.* **36**, 2585 (2006).
27. The time (*y*, years) required for a semi-arid forest to achieve balance between the surface positive *RF* and the carbon sequestration negative *RF* is approximated based on (*17*) as $y = \left(\frac{RF_{surface} \cdot \kappa \cdot C_0}{A_E \cdot NEE \cdot \eta \cdot \zeta}\right)$, where $RF_{surface}$ is either the albedo or the combined albedo-longwave effect, RF_{s+L}, A_E the Earth surface area (m^2), κ converts parts per million (ppm) CO_2 to kg C, C_0 the reference atmospheric CO_2 concentration (370 ppm), η is the CO_2 radiative forcing efficiency (W m^{-2}), ζ is the airborne fraction, and *NEE* is the observed annual net carbon uptake of the semi-arid forest (kg C m^{-2} $year^{-1}$).
28. E. L. Davin, N. de Noblet-Ducoudre, P. Friedlingstein, *Geophys. Res. Lett.* **34**, L13702 (2007).
29. H. N. Le Houérou, *J. Arid Environ.* **34**, 133 (1996).
30. S. Pacala, R. Socolow, *Science* **305**, 968 (2004).
31. G. P. Asner, J. M. O. Scurlock, J. A. Hicke, *Glob. Ecol. Biogeogr.* **12**, 191 (2003).
32. J. F. Reynolds *et al.*, *Science* **316**, 847 (2007).
33. Food and Agriculture Organization (FAO), *Carbon Sequestration in Dryland Soils* (World Soils Resources Reports 102, FAO, Rome, 2004).
34. J. G. Canadell *et al.*, *Proc. Natl. Acad. Sci. U.S.A.* **104**, 18866 (2007).
35. www.esrl.noaa.gov/gmd/ccgg
36. http://gaia.agraria.unitus.it/database/carboeuropeip/
37. W. J. Shuttleworth *et al.*, *Q. J. R. Meteorol. Soc.* **110**, 1163 (1984).
38. W. Knorr, K. G. Schnitzler, Y. Govaerts, *Geophys. Res. Lett.* **28**, 3489 (2001).
39. T. T. Warner, *Desert Meteorology* (Cambridge Univ. Press, Cambridge, 2004).
40. G. S. Campbell, J. M. Norman, *An Introduction to Environmental Biophysics* (Springer-Verlag, New York, ed. 2, 1998).
41. V. Masson, J. L. Champeaux, F. Chauvin, C. Meriguet, R. Lacaze, *J. Clim.* **16**, 1261 (2003).
42. J. Peixoto, A. Oort, *Physics of Climate* (Springer-Verlag, New York, 1992).
43. S. Luyssaert *et al.*, *Glob. Change Biol.* **13**, 2509 (2007).
44. T. Afik, thesis, Hebrew University of Jerusalem (2009).
45. R. H. Shaw, A. R. Pereira, *Agric. Meteorol.* **26**, 51 (1982).

46. We thank the students, postdocs, and technicians of the Yatir team for making this project possible. The long-term operation of the Yatir Forest Research Field Site is supported by the Cathy Wills and Robert Lewis Program in Environmental Science. Financial support from the Israel Science Foundation, Global Change and the Hydrological Cycle–Jordan River (GLOWA-JR), Keren Kayemet L'Israel (KKL), Jewish National Fund (JNF), the Minerva-Avron Center, and the Weizmann Institute is gratefully acknowledged.

31 July 2009; accepted 28 December 2009
10.1126/science.1179998

Downloaded from www.sciencemag.org on November 23, 2012

Modeled Impact of Anthropogenic Warming on the Frequency of Intense Atlantic Hurricanes

Morris A. Bender,[1]* Thomas R. Knutson,[1] Robert E. Tuleya,[2] Joseph J. Sirutis,[1] Gabriel A. Vecchi,[1] Stephen T. Garner,[1] Isaac M. Held[1]

Several recent models suggest that the frequency of Atlantic tropical cyclones could decrease as the climate warms. However, these models are unable to reproduce storms of category 3 or higher intensity. We explored the influence of future global warming on Atlantic hurricanes with a downscaling strategy by using an operational hurricane-prediction model that produces a realistic distribution of intense hurricane activity for present-day conditions. The model projects nearly a doubling of the frequency of category 4 and 5 storms by the end of the 21st century, despite a decrease in the overall frequency of tropical cyclones, when the downscaling is based on the ensemble mean of 18 global climate-change projections. The largest increase is projected to occur in the Western Atlantic, north of 20°N.

Rising sea-surface temperatures (SSTs) and a possible increase in Atlantic basin hurricane activity since 1950 have raised concern that human-caused climate change may be increasing Atlantic hurricane activity. Increasing amounts of greenhouse gases are a likely factor in the recent warming of tropical Atlantic SSTs (*1*–*3*), although internal variability (*4*) and reduced aerosol or dust forcing (*5*, *6*) may have also contributed. Some statistical analyses suggest a link between warmer Atlantic SSTs and increased hurricane activity (*6*–*8*), although other studies contend that the spatial structure of the SST change may be a more important control on tropical cyclone frequency and intensity (*9*–*11*). A few studies (*6*, *8*, *12*) suggest that greenhouse warming has already produced a substantial rise in Atlantic tropical cyclone activity, but others question that conclusion (*9*, *11*, *13*).

Dynamical models that can reproduce certain aspects of the observed frequency, structure, and intensity of hurricanes bring an important perspective to these questions (*9*, *10*, *14*–*16*). A recent modeling study (*16*) at the National Oceanic and

[1]National Oceanic and Atmospheric Administration/Geophysical Fluid Dynamics Laboratory, 201 Forrestal Road, Princeton, NJ, 08540, USA. [2]Center for Coastal Physical Oceanography, Old Dominion University, 4111 Monarch Way, Norfolk, VA 23508, USA.

*To whom correspondence should be addressed. E-mail: Morris.Bender@noaa.gov